Sea-Breeze Convergence Zones from AVHRR over the Iberian Mediterranean Area and the Isle of Mallorca, Spain

CESAR AZORIN-MOLINA

Laboratory of Meteorology and Climatology, Mixed Unity CEAM-UVEG, The CEAM Foundation (Fundación Centro de Estudios Ambientales del Mediterráneo), Paterna, Valencia, and Group of Climatology, University of Barcelona, Barcelona, Spain

BERNADETTE H. CONNELL

Cooperative Institute for Research in the Atmosphere, Colorado State University, Fort Collins, Colorado

RAFAEL BAENA-CALATRAVA

High Technical College, University of Jaen, Jaen, Spain

(Manuscript received 9 October 2008, in final form 23 April 2009)

ABSTRACT

The aim of this study was to identify clear air boundaries and to obtain spatial distribution of convective areas associated with the sea breeze over the Iberian Mediterranean zone and the isle of Mallorca, both in Spain. Daytime Advanced Very High Resolution Radiometer (AVHRR) data from National Oceanic and Atmospheric Administration (NOAA) polar-orbiting satellites were collected for May–October 2004. A cloud detection algorithm was used to identify clouds to derive daytime sea-breeze cloud frequency composites over land. The high-resolution composites aided in identifying the location of five preferential sea-breeze convergence zones (SBCZ) in relation to the shape of coastline and orographic effects. Additionally, eight regimes were designated using mean boundary layer wind speed and direction to provide statistics about the effect of prevailing large-scale flows on sea-breeze convection over the five SBCZ. The offshore SW to W and the NW to N regimes were characterized by high cloud frequencies parallel to the coast. Small differences in mean cloud frequency values from morning to afternoon composites were detected with these regimes because sea-breeze fronts tended to form early and persist into the afternoon. Just the opposite occurred under the onshore NE to E and SE to S regimes. It was found that light to moderate ($\leq$5.1 m s^{-1}) winds aloft result in more clouds at the leading edge of sea breezes. In contrast, strong synoptic-scale ($>$5.1 m s^{-1}) flows weaken boundary layer convergence. The results from this satellite meteorology study could have practical applications for many people including those that forecast the weather and those that use the forecast for making decisions related to energy use, fishing, recreation, or agriculture activities, as well as for estimating pollution or issuing warnings for heavy rain or flash flooding.

1. Introduction

The high-resolution visible (VIS) and infrared (IR) satellite imagery composites are powerful tools for observing the timing, location, and intensity of convection associated with sea-breeze fronts (e.g., Connell et al. 2001). Sea-breeze complex interactions (e.g., Simpson 1994), as exemplified by the features of the coastline, the small-scale terrain, and the large-scale flows, make the short-term forecast difficult (e.g., González Márquez and Heredia 2001). The Forecast and Security Group (GPV) of the Spanish Meteorological Agency (AEMET) use the following tools for nowcasting the location and strength of the sea-breeze convergence zones (SBCZ): (i) numerical model outputs, (ii) sounding data, and (iii) three stability indices: total totals (TOTL; $>$45), convective available potential energy (CAPE; $>$0), and lifted index (LIFT; $<$0), derived from sounding data. The short-term forecast of the timing, location, and intensity of sea-breeze convection is difficult. Thunderstorms are challenging to predict because they usually develop under

Corresponding author address: Cesar Azorin-Molina, Fundación Centro de Estudios Ambientales del Mediterráneo, Parque Tecnológico, Charles R. Darwin 14, 46980-Paterna (Valencia), Spain. E-mail: cazorin@ceam.es

DOI: 10.1175/2009JAMC2141.1

weakly defined synoptic-scale or mesoscale precursor disturbances (e.g., Wilson et al. 2007). The SBCZ can provide enough energy to overcome the stable cap of the boundary layer and generate local showers and thunderstorms. González-Márquez and Heredia (2001) reported a summer sea-breeze convective episode on the isle of Mallorca with TOTL = 42 and CAPE = 0 that produced 24 mm of precipitation.

The complex interactions of the sea breeze can be studied by analyzing cloud patterns in satellite imagery. The high-resolution satellite imagery gives a unique view of the SBCZ and convective activity (e.g., Purdom 1976; Koch and Ray 1997). Sea-breeze fronts are defined by a cloud line parallel to the coastline. The width of the cloud-free zone produced by the sinking motion on the seaward side of the circulation depends on the inland propagation of sea-breeze fronts. Azorin-Molina et al. (2009) concluded that the primary effect of sea breezes on cloud genera is to increase the frequency of low [stratus (St)] and convective [cumulus (Cu)] clouds, and this local wind triggers the formation of thunderstorms clouds [cumulonimbus (Cb)] at the SBCZs. The satellite imagery often shows a line of larger convective clouds (cumulus and cumulonimbus clouds) at the leading edge of the low-level onshore component, where convergence and vertical motion are enhanced under an unstable or neutrally stable environment (e.g., Arritt 1993). The cumuliform cloud line on a cloudless sky represents the sea-breeze front, which is like a miniature cold front (e.g., Strickler 2003) separating the land and sea air. Sea-breeze fronts are the prime location for convective development and therefore can cause small fair-weather Cu or local thunderstorms with heavy precipitation (rain or hail) in inland areas not far from the coast. During the summer dry season, this is typically the only source of precipitation in this area (Olcina-Cantos and Azorin-Molina 2004), bringing an average of 100–125 mm yearly to inland areas (Millán et al. 2005).

Most air boundaries that cause storm development are primarily associated with the sea breeze, since they are the main mesoscale circulation in terms of occurrence and persistence over the region. Consequently, sea-breeze fronts are common phenomena from May to October in the Iberian Mediterranean area and the isle of Mallorca (Spain; Fig. 1a). Despite their importance for local weather and climate, as well as for glider pilots and environmental scientists interested in the distribution of airborne pollution (e.g., Simpson 1994), sea-breeze fronts have been sparsely studied over the study area. Based on an inquiry made among farmers and fishermen, Jansà and Jaume (1946) showed a pioneering map of SBCZ produced by the β-mesoscale circulation and the γ-mesoscale eddies caused by the topography on the isle of Mallorca. Ramis and Alonso (1988) used geostationary visible imagery on 11 May 1987 to show the development of the SBCZ in the center of the isle. Terradelles (1997) used lightning data and Pascual (1999) used geostationary infrared imagery to develop convection climatologies in Catalonia [northeastern Iberian Peninsula (IP)]. Pascual et al. (2004) examined polar 1.1-km VIS and IR satellite imagery from *NOAA-16* and *-17* to infer the existence of boundary layer convergence lines for sea breeze and coastal range interaction in Catalonia. Radar data have also been used to study planetary boundary layer convergence zones (e.g., Wilson and Schreiber 1986; Pascual and Callado 2002; Callado and Pascual 2002; Pascual et al. 2004). As a result of previous field campaigns, Olcina-Cantos and Azorin-Molina (2004) put forward a conceptual classification of sea-breeze fronts based on (i) stable conditions associated with tropical air masses and (ii) unstable conditions associated with polar air masses in relation to the development of St and Cu clouds or scattered locally heavy showers and thunderstorms, respectively.

The first research on high-resolution cloud frequency composites related to large-scale flows and small-scale geographic features was developed by Klitch et al. (1985) and Gibson and Vonder Haar (1990). Gould and Fuelberg (1996) and Connell et al. (2001) focused their investigations on the sea-breeze cloud climatology over the Florida Panhandle. Their results are being used in short-range forecasts for meteorology, maritime, and aviation applications. Damato et al. (2003) and Planchon et al. (2006) employed *NOAA-14* and *GOES-8* data, respectively, and used a technique based on screen digitizing to create cartography of the occurrence, location, and inland penetration of sea-breeze fronts in the English Channel and in northeastern Brazil.

This paper provides the first sea-breeze cloud frequency composites over the Iberian Mediterranean area and the isle of Mallorca. The remote sensing study has been designed to offer quantitative and high-quality composites of frequently occurring SBCZ in relation to the regional-scale atmospheric circulation, the shape of the coastline, and the small-scale geographic features. Most of the time, cloud frequency is presented in the form of a monthly or seasonal composite. When the imagery are stratified based on a particular variable such as the background wind, the result is a better depiction of synoptic influences that produce a particular cloud distribution. It is often important to know where clouds are likely to develop as well as less likely to develop. This may have intuitively been known beforehand, but now there is evidence in the cloud field. It is more informative than that given by a point surface observation of overhead cloud cover. It is expected that during any

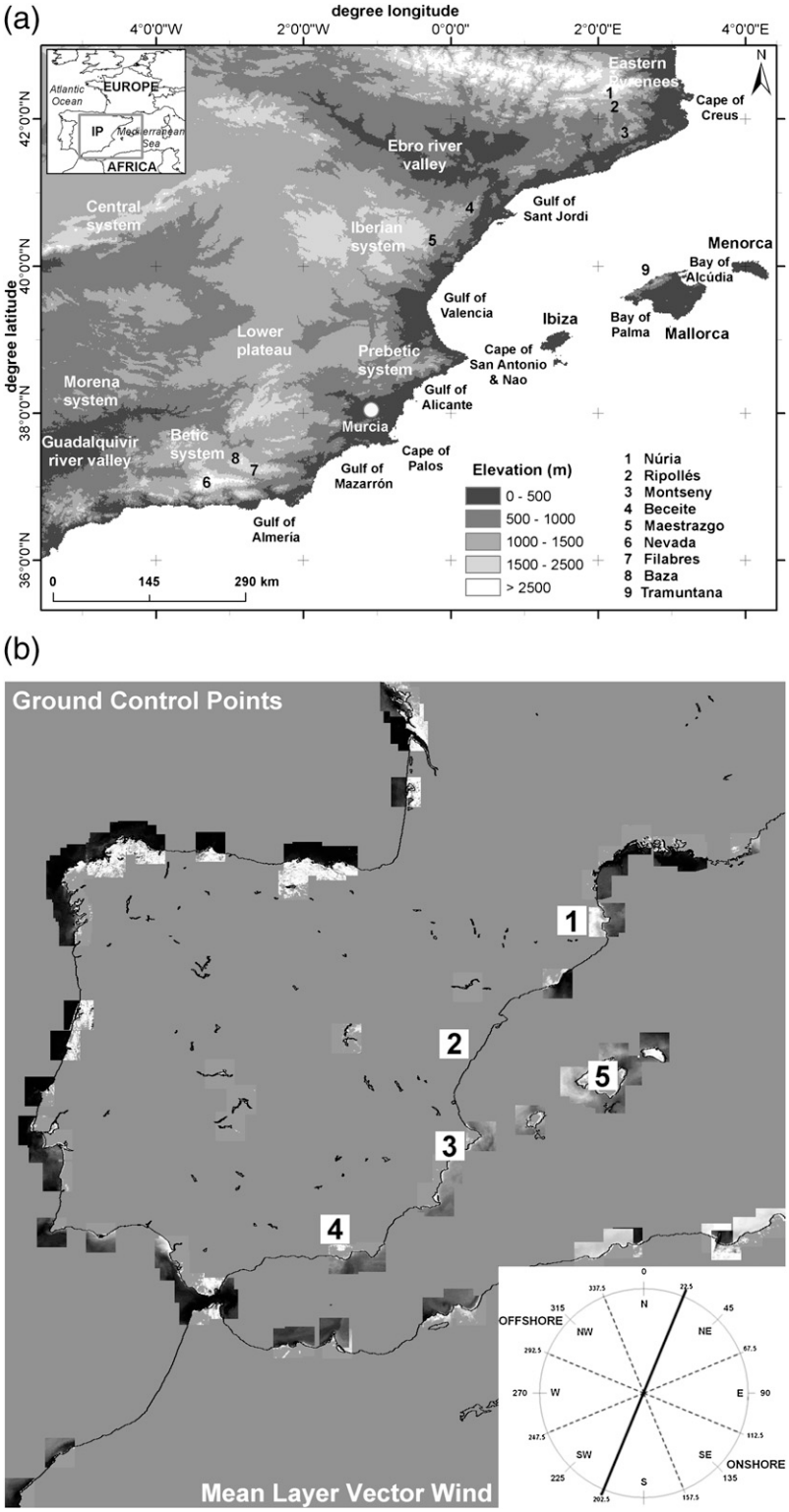

FIG. 1. (a) Map of the study area showing locations named in the text. The white circle represents the rawinsonde upper-air sounding location at Murcia. (b) GCPs used for a second geometric correction. Wind direction (WD) of the MLVW regimes is given in the lower right corner. White squares are arrays of 50 × 50 pixels centered over the five frequently occurring SBCZ for computing basic statistics in section 3.

given year, different types of weather patterns will be encountered over a region. The frequency of occurrence of a particular pattern will, however, vary from month to month, season to season, and year to year. Even though this study looks at one period of data, it captures representative cloud frequency patterns for different background wind regimes applicable on regional and local scales. Information from this one time period can be used to tailor further long-term studies that utilize cloud frequencies.

Another motivation for studying the spatial distribution of convective areas associated with the sea breeze is to gain better knowledge on the severe thunderstorm development, which could have applications for short-term forecasts. Severe and moderate thunderstorm events can occur under sea-breeze situations, even though weather reports forecast mostly clear skies. Pascual et al. (2004) concluded that ''knowledge of areas where convection develops most frequently (hot spots) is a first step toward obtaining accurate nowcasts.''

2. Data and methods

a. AVHRR and preprocessing data

Advanced Very High Resolution Radiometer (AVHRR) data from the National Oceanic and Atmospheric Administration (NOAA) polar-orbiting satellites were used for deriving sea-breeze cloud frequency composites. AVHRR full-horizontal-resolution data (1.1 km) from *NOAA-17* morning (0900–1200 UTC) and *NOAA-16* afternoon (1200–1500 UTC) orbits were collected from the High Resolution Picture Transmission (HRPT) receiving ground station placed at the National Institute for Aerospace Technology (INTA; Mas Palomas, Canary Isles, Spain; http://www.inta.es/), for the warm 6-month period of May–October 2004. The 1.1-km spatial resolution at nadir of the AVHRR imagery is useful in finding SBCZ because it is close to the Cu cloud scale. In addition, the morning and afternoon orbits capture the early convective stages (small-scale Cu clouds) and maximum deep convection (Cb clouds), respectively.

A fully automated pixel-by-pixel preprocessing routine using the header files (metadata) of L1B data (binary file) was designed in Environment for Visualizing Images (ENVI) + Interactive Data Language (IDL) 4.2 package following the project carried out by Baena-Calatrava (2002). The routine included radiometric calibration for five channels, as well as calculation of satellite zenith and solar zenith angles for each point. The solar channels 1 (0.58–0.68 μm) and 2 (0.72–1.10 μm) were calibrated to reflectance (in percent) and the thermal IR spectrums 4 (10.30–11.30 μm) and 5 (11.50–12.50 μm) to brightness temperature (K). Since channel 3b (3.55–3.93 μm) from the *NOAA-16* satellite is always on (no 3a switching) it was calibrated to brightness temperature (K). However, the *NOAA-17* satellite switches channels at the terminator such that 3a (1.58–1.64 μm) is on during daylight and 3b is on during night. Therefore, channel 3a from *NOAA-17* was calibrated to reflectance (in percent). No procedures to normalize VIS and IR AVHRR radiances were applied, and therefore the cloud detection process described below is assumed to be slightly sensitive to errors in calibration for both *NOAA-16* and *NOAA-17* measurements as evaluated by Roebeling et al. (2006). Nevertheless, these five AVHRR channels helped to better delineate between cloud, snow–ice, and clear ground pixels to obtain the cloud amount. The routine in IDL also included a geometric correction to the European 1979 UTM-zone 30°N coordinate system over an area bounded between 32°20′ and 46°46′N and 13°15′W and 6°47′E. A second automatic geometric correction technique taking a set of 97 ground control points (GCPs; Fig. 1b) (Ho and Asem 1986; Brush 1988; Bachmann and Bendix 1992; Moreno and Meliá 1994; Parada et al. 2000) along the coastline of southwestern Europe and the northern African continent was also applied to improve the registration of the output data.

The cloud frequency composites presented here only looked at pure convective development associated with the sea breeze. A set of three mixed objective–manual criteria similar to Wilson et al. (2007) were applied to detect true sea-breeze boundaries and reject active synoptic-scale or mesoscale disturbances. The first criterium focused on selection of favorable synoptic environments using Jenkinson and Collison (1977) weather type classification (i.e., anticyclonic circulation, thermal lows over the IP, or weak surface pressure gradients). The second criterion of temperatures $\geq$20°C in the planetary boundary layer ensured enough surface heating to provide convection. Under the third criteria, large-scale flows (mean layer vector wind between 1000 and 700 hPa) <13 m s^{-1} (e.g., Savijärvi and Alestalo 1988; Arritt 1993; Kwiatkowski 1999) allowed for the sea breeze to develop. Those days that met criteria 1–3 were visually screened. Images that showed a line of larger Cu and Cb clouds at the leading edge of the sea breeze on a cloudless sky were selected. Convection embedded in multilevel cloud cover was rejected (i.e., the manual selection visually screened out high-, medium-, and low-cloud cases where we could not detect a characteristic line of Cu and Cb clouds associated with the sea-breeze front development). A set of 69 and 76 images from *NOAA-17* and *NOAA-16*, respectively, were used (Table 1). Although the study covered May–October 2004, June, July, and August accounted for 65.2% of *NOAA-17* and 61.8% of *NOAA-16* imagery.

TABLE 1. Number of *NOAA-17* and *-16* images for the 6-month study period May–October 2004.

Satellite	May	Jun	Jul	Aug	Sep	Oct	Total
NOAA-17	9	13	18	14	8	7	69
NOAA-16	8	15	19	13	13	8	76

b. An automated cloud detection algorithm

The cloud detection algorithm has been based on the AVHRR Processing Scheme over Clouds, Land and Ocean (APOLLO), which was developed by Saunders (1986) and Saunders and Kriebel (1988). APOLLO was designed to process AVHRR HRPT data as well as local area coverage (LAC) and global area coverage (GAC) data over western Europe and the North Atlantic. This cloud analysis tool has been modified and extended by others (e.g., Derrien et al. 1993; Karlsson 1996; Stowe et al. 1999; Kriebel et al. 2003). A daytime over land algorithm (solar elevation greater than 5°) is presented for computing sea-breeze cloud detection over the IP and the isle of Mallorca for both *NOAA-17* (morning pass) and *NOAA-16* (afternoon pass) AVHRR data. The daytime over land algorithm that was used to derive sea-breeze cloud composites consists of four spectral tests applied to each pixel. The constant thresholds have been successfully tested to be functional during the 6-month study period of May–October.

Test 1 corresponds to snow–ice detection. Snow can be discriminated from cloud using visible and shortwave infrared channels. For *NOAA-17*, a quota ratio (Q1) is defined as the ratio of reflectance of 1.6 μm divided by the reflectance of 0.6 μm. Since snow is considerably less reflective at 1.6 μm, values of Q1 $\leq$ 0.2 designate a snow–ice pixel. We used a threshold brightness temperature difference (BTD) of $\leq$15 K between 3.7 and 11 μm for detecting snow–ice pixels for *NOAA-16*. May, June, and October have snow–ice pixels over the Pyrenees, the Iberian System, and the Betic Mountains within the study area.

Test 2 is the IR gross threshold test at 12 μm. A unique threshold of $\leq$290 K was used to select cloudy pixels representing all cloud types for both satellites. Sea-breeze fronts develop under high insolation and therefore land surface temperatures during the day (LST) are >290 K even during the cooler months.

Test 3 is the albedo or visible test at 0.6 μm. A fixed threshold reflectance of $\geq$20% was chosen to select cloudy pixels.

Test 4 is the reflectance quotient (Q2) of near-IR ($R_{0.9\mu m}$) to VIS ($R_{0.6\mu m}$). A Q2 threshold from 0.7 to 1.3 identified cloudy pixels. A supplementary IR threshold test was added to discriminate bare ground pixels from cloudy ones. We tagged as cloudy the pixels with a Q2 ratio between 0.7 and 1.3 and $T_{12} \leq 290$ K.

The algorithm discretizes all AVHRR data into three groups: cloud-free, cloudy, and snow–ice. The algorithm identifies a pixel as cloudy if at least two tests (test 2, 3, or 4) prove positive. The final cloud determination is obtained by subtracting snow–ice pixels from cloudy ones. A detailed description of the accurate high-resolution cloud detection algorithm is presented and discussed by Azorin-Molina et al. (2007a).

c. Low-level synoptic flow regimes, coastline shape typology, and image compositing

The AVHRR data have been used together with other sources of mesoscale meteorological information (e.g., Pautz 1971; Purdom 1976; Gould and Fuelberg 1996): the direction and strength of low-level synoptic flow and the shape of coastline have been addressed here.

The low-level wind field and the frictional effects produced by the terrain (e.g., Petterssen 1956) cause convergence and local sea-breeze front intensification. The prevailing low-level boundary layer wind has been shown to be the most influential factor on sea-breeze evolution (e.g., Estoque 1962; Blanchard and López 1985; Bechtold et al. 1991; Gould and Fuelberg 1996; Connell et al. 2001). Upper-air observations recorded at Murcia (station 80430, southeastern IP; Fig. 1a) were used for computing mean layer vector wind (MLVW) from 1000 to 700 hPa at 1200 UTC. Surface wind data were not employed since they may contain mesoscale contamination (e.g., Gould and Fuelberg 1996). This specific rawinsonde observation point is representative of large-scale ambient flow over the whole study area.

The MLVW regime classification is summarized in Table 2. The SW to W flow (regimes 5 and 6) occurs 40.6% (*NOAA-17*) and 43.4% (*NOAA-16*) of the time; NW to N flow (regimes 7 and 8) is the next most frequently occurring regime (*NOAA-17*: 29.0% and *NOAA-16*: 32.9%). The SE to S flow (regimes 3 and 4) is third (*NOAA-17*: 15.9% and *NOAA-16*: 13.2%), and NE to E winds (regimes 1 and 2) occur less frequently (*NOAA-17*: 14.5% and *NOAA-16*: 10.5%). The percentage differences between *NOAA-17* and *NOAA-16* for each of the classifications are due to (i) missing AVHRR data and (ii) the selection of images presented in the section 2a. The categories do not fall into strict onshore and offshore flow regimes because the shape of the coastline is variable. Nevertheless, note that regimes 1–4 and 5–8 are more or less onshore and offshore flows, respectively, due to the general SW–NE shoreline orientation of the Iberian Mediterranean coast. For the isle of Mallorca, regimes 1–4 are almost onshore and offshore

TABLE 2. MLVW regimes and number of days (or images) designated for each wind speed (WS) regime for the 6-month study period May–October 2004.

Regime	WD	WS (m s^{-1})	*NOAA-17* (No. of images)	*NOAA-16* (No. of images)
1	NE–E (22.6°–112.5°)	≤5.1	6	6
2		>5.1	4	2
3	SE–S (112.6°–202.5°)	≤5.1	7	5
4		>5.1	4	5
5	SW–W (202.6°–292.5°)	≤5.1	12	14
6		>5.1	16	19
7	NW–N (292.6°–22.5°)	≤5.1	11	14
8		>5.1	9	11

for the eastern and western half the isle, respectively, and just the opposite for regimes 5–8.

Onshore flows greater enhance the inland penetration and the earlier onset of sea breeze than offshore flows. Furthermore, the convergence of sea breezes is not well defined under onshore regimes, whereas offshore flows sharpen the leading edge of sea breezes and a pronounced discontinuity and convergence intensification result (e.g., Wakimoto and Atkins 1994; Strickler 2003). The regimes are divided into light–moderate intensities (≤5.1 m s^{-1}) and strong wind speeds (>5.1 m s^{-1}). Sea-breeze fronts developed between 2.1 and 9.1 m s^{-1}. Synoptic-scale flows aloft between 4.1 and 5.1 m s^{-1} have been found to be the most frequent velocities for sea-breeze front development. Strickler (2003) found that the largest upward vertical velocity along the discontinuity occurs for the strongest offshore flows that still allow sea breezes.

The coastline shape enhances or reduces convergence, vertical motion, and convective distribution along sea-breeze fronts (e.g., Neumann 1951; Pielke 1974; Strickler 2003). On a convex coastline (i.e., peninsulas, capes, points, and also islands), sea breezes become convergent, enhancing convergence, increasing uplift processes, and strengthening earlier cumulus activity and thunderstorms along the frontal area. Sea-breeze flows from opposing coastlines produce merging convective cells near the center of peninsulas and islands. On a concave land–water boundary (bays and inlets) just the opposite occurs (e.g., Purdom 1976), inhibiting strong upward vertical velocity required for convective development (e.g., Strickler 2003). McPherson (1970) and Purdom (1976) pointed out that the unevenness of coastlines also plays a relevant role in the convective development along sea-breeze fronts. Figure 1a displays the main features of the shoreline along the Iberian Mediterranean coast and the isle of Mallorca.

Sea-breeze cloud frequency composites were computed for the period May–October, as well as for monthly and MLVW regimes. The results are presented in section 3 for both morning and afternoon orbits. The cloud frequency maps were based on the cloud count for a pixel-by-pixel basis and were calculated as follows:

$$f_i = \frac{n_i}{N} 100, \tag{1}$$

where n_i is the count of cloudy pixels and N is the total number of selected scenes, and the results were multiplied by 100. The averaged cloud composite for a given satellite, month, and regime is not based on the same number of input images.

To compare cloud frequency between morning and afternoon composites, the mean cloud frequency values (%) for a 50 × 50 pixel array centered over the maximum cloud frequency zone for each SBCZ were computed. The 50 × 50 pixel array size covers a large enough area to compute cloud frequency statistics, as it is shown in Fig. 1b.

d. May–October 2004 weather summary

The mean monthly sea level pressure field [National Centers for Environmental Prediction–National Center for Atmospheric Research (NCEP–NCAR) reanalysis map; Kalnay et al. 1996] was characterized by a high presence of the Iberian thermal low and a weak gradient around eastern Spain and the western Mediterranean basin. Generally, the summer climatology was characterized by temperatures above mean over land surfaces and therefore greater land–sea air temperature differences, which allowed development of the sea breeze. Precipitation was above the mean in May, June, and July (particularly in the northeastern IP and the isle of Mallorca), and below the mean in August, September (except in the Valencia region and southern part of Catalonia), and October (INM 2004, 2005). Thunderstorm reports were frequent in May–August (northeastern IP and the isle of Mallorca).

3. Results

a. May–October cloud frequency composites and SBCZ

Figure 2 shows May–October sea-breeze cloud frequency maps over an area bounded between 35°32′ and 42°48′N and 5°56′W and 4°42′E for the morning (Fig. 2a)

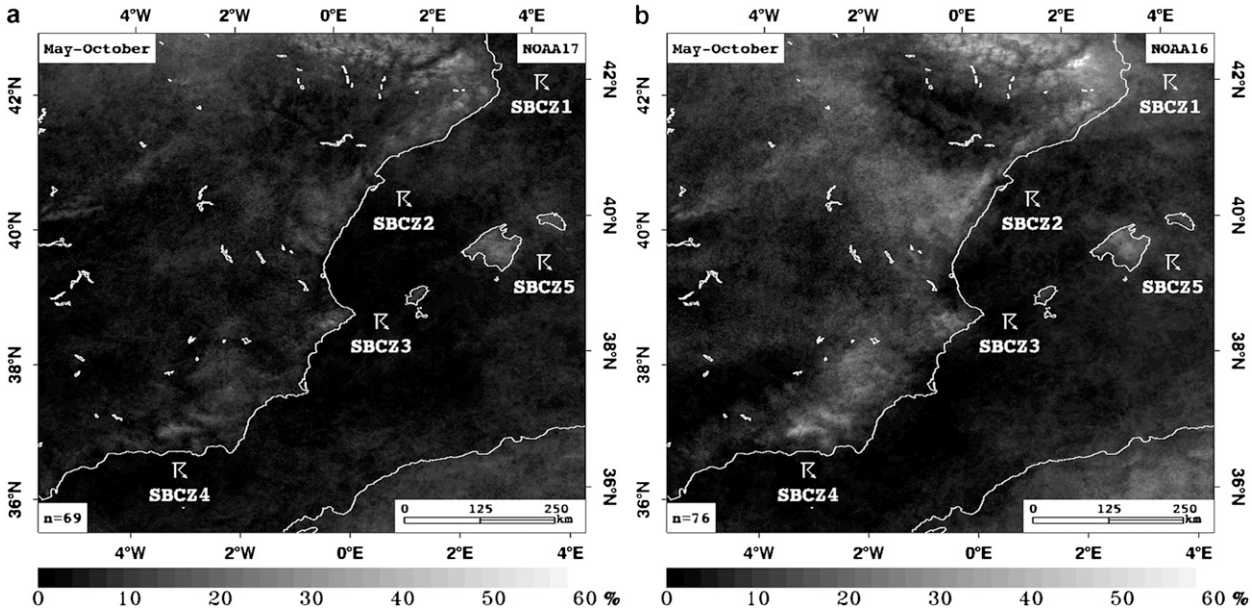

FIG. 2. Sea-breeze cloud frequency composites for (a) morning (*NOAA-17*) and (b) afternoon (*NOAA-16*) orbits during the 6-month study period: May–October 2004. The number of images averaged is shown in the lower-left corner of each image (n = sample size). The thunderstorm symbols indicate location of the five prominent SBCZ. Note that the grayscale ranges in frequency from 0% to 60% to highlight SBCZ.

and afternoon (Fig. 2b) orbits. Both of these overall high-resolution composites are very good at depicting the location of the frequently occurring SBCZ in relation to the shape of coastlines and topography. We found five preferential areas along the sea-breeze front with higher convective activity as shown by increased cloud frequency over surrounding areas. The regions of increased cloud frequencies (with >30% or more maximum cloud frequency) are referred to as convective hot spots and are as follows:

1) The SBCZ1 corresponds to the eastern Pyrenees and pre-Pyrenees ranges (Vall de Núria and Ripollés mountains) in northeastern IP. This is an important planetary boundary layer convergence zone with afternoon maximum cloud frequencies ranging from 50.0% to 60.0%. The two prelittoral mountain ranges (Montseny mountains), which extend NE to SW parallel to the coast (10 km from the shoreline), are also noteworthy with afternoon maximum cloud frequency values above 40.0%. This is due to the complex interactions between the sea breeze, which moves inland (e.g., Pascual et al. 2004), supplying moisture from the Mediterranean Sea, and the varied orography—upvalley–upslope winds (Lana et al. 1995; Martínez et al. 2007)—with an average elevation of 1500–3000 m. Convergence processes associated with the convex coastline in northeastern IP (Cape of Creus) also contribute to increased convection in this region. Note that the hot spot is associated with the convex portion of the coastline. Pascual and Callado (2002) also recognized this SBCZ as a planetary boundary layer convergence area associated with sea breeze–coastal range interactions. Callado and Pascual (2005) reported an interesting convective storm associated with sea-breeze fronts over the Mediterranean Pyrenees and near-coastal region on 26 August 2003; the maximum rainfall was 35–40 mm. The mean cloud frequencies computed from an array of 50 × 50 pixels centered over the maximum cloud frequency zone are the highest for all groups with 18.4% (*NOAA-17*) and 32.3% (*NOAA-16*).
2) The SBCZ2 includes the eastern region of the Iberian system mountains and has afternoon maximum cloud frequencies above 35.0% for the Maestrazgo Mountain range and 30.0% for the Puertos de Beceite Mountain range. The region with 30%–35% frequency is between 15 and 30 km wide and stretches a parallel thin line about 125 km (from SSW to NNE) along the coast. The SBCZ2 follows the ridge of the coastal mountain ranges (which is on average 20–25 km inland). The mountainous topography (1000–1900 m) and the concave coastal features to the north (Gulf of Sant Jordi) and to the south (Gulf of Valencia) also enhance sea-breeze convergence. The sea-breeze storms tend to form

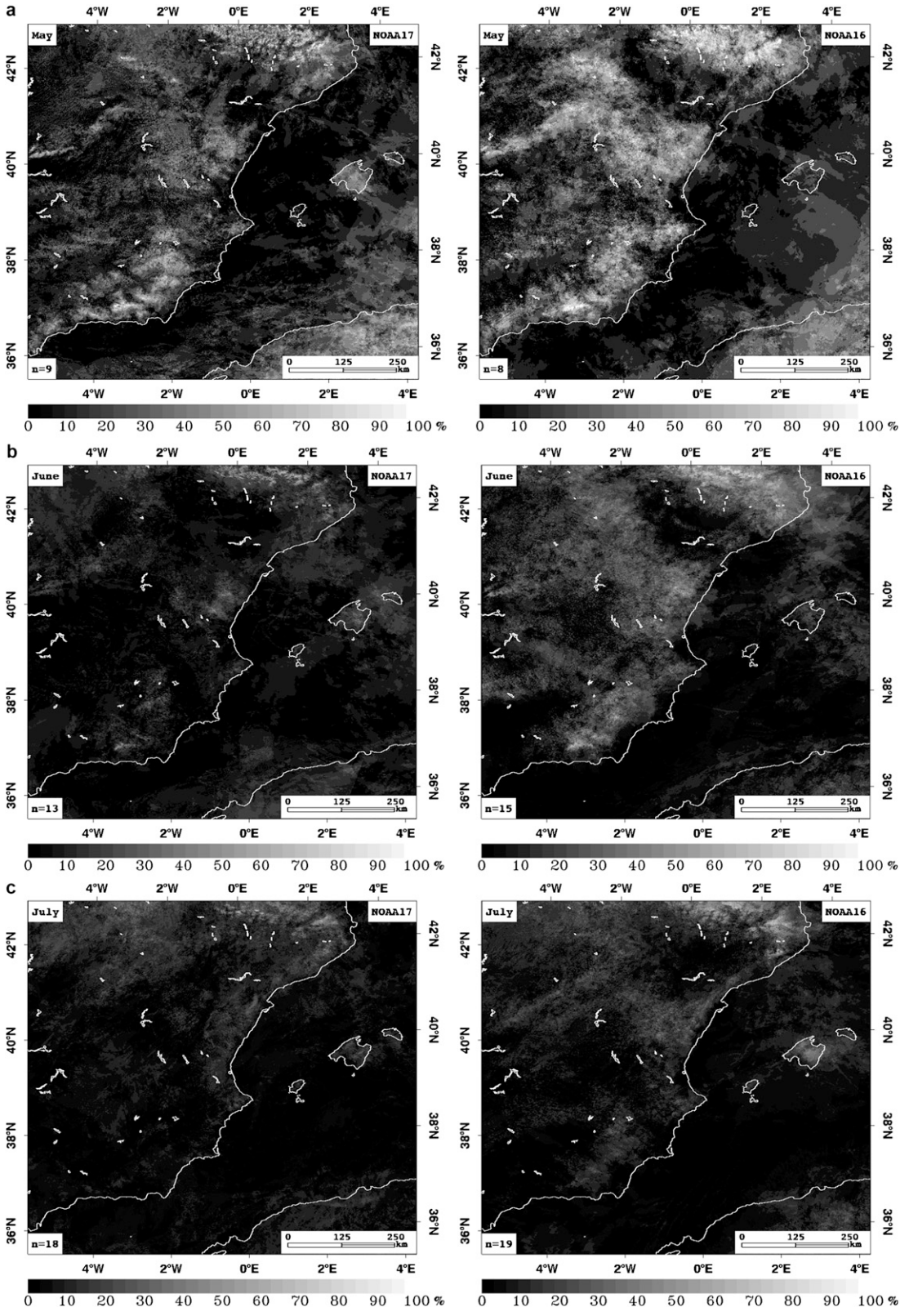

FIG. 3. As in Fig. 2, but for morning and afternoon composites during (a) May, (b) June, (c) July, (d) August, (e) September, and (f) October.

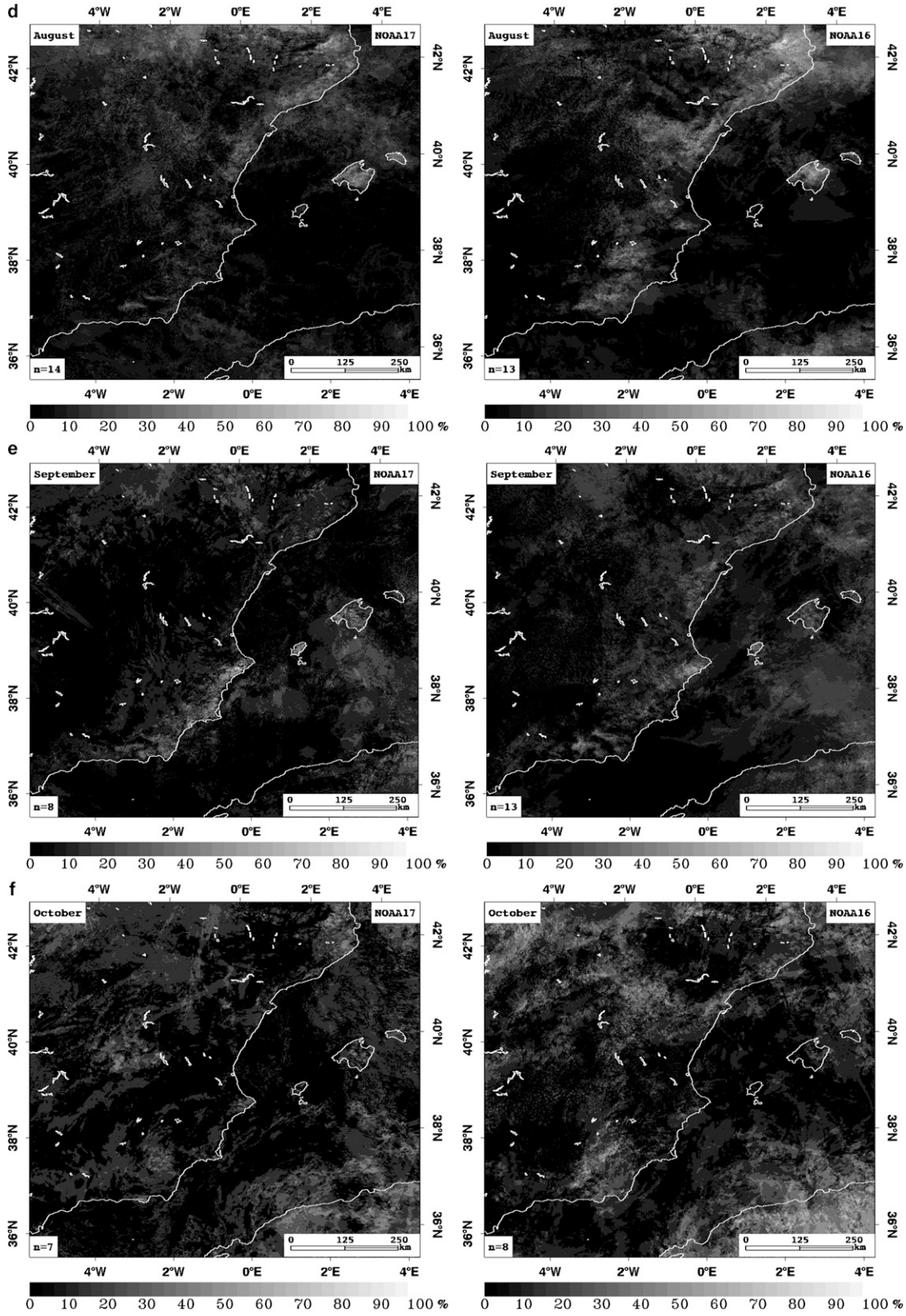

FIG. 3. (*Continued*)

on the east- and south-facing slopes of the coastal mountain ranges in mid–late afternoon (Millán et al. 2005). This is due to the early onset of solar heating and strongest boundary layer circulations developed along the Mediterranean coast. In addition, the slope angle is more important than terrain height in forming convection (Klitch et al. 1985). Note that there is lower cloud cover (10%–25%) over the Iberian system mountains that are further inland (i.e., far from the influence of Mediterranean sea breezes). Unlike the general minima of rainfall in summertime over the Mediterranean basin, the SBCZ1 and SBCZ2 have local maxima of precipitation at this season (e.g., Martín-Vide and Olcina-Cantos 2001; Callado and Pascual 2005), which support these results. The mean cloud amounts from an array of 50 × 50 pixels are 11.7% (*NOAA-17*) and 21.8% (*NOAA-16*).

3) The SBCZ3 is a small region that contains the Prebetic mountain ranges (1000–1600 m) in Alicante. It has afternoon maximum cloud frequency amounts above 30.0%. The convex coastline (Cape of Sant Antoni and Cape of Nao) along the Iberian Mediterranean coast strengthens the Cu activity over the zone. This is a locally well-known convective hot spot. Azorin-Molina (2002) analyzed the development of a convective storm under sea-breeze conditions over the Prebetic mountain ranges on 27 April 2001, and reported exceptional episodes of more than 150 mm of precipitation. The mean cloud frequencies from an array of 50 × 50 pixels are 7.5% (*NOAA-17*) and 14.1% (*NOAA-16*).
4) The SBCZ4 is collocated with the Betic system mountains (Nevada, Filabres, and Baza mountain ranges; 2000–3500 m) with afternoon maximum cloud frequency values above 35.0%. The convergence zone and the growth of Cu clouds is enhanced as the day progresses and sea breezes and anabatic winds on heated mountain slopes interact, strengthening uplift processes. Millán et al. (2005) concluded that summer storms are associated with the final stages of development of the combined sea breezes and upslope winds. This has been documented in some European research projects (Millán et al. 1996, 1997). The mean cloud amounts from an array of 50 × 50 pixels are 8.1% (*NOAA-17*) and 17.9% (*NOAA-16*).
5) The SBCZ5 corresponds to the isle of Mallorca in the Balearic archipelago. Sea-breeze flows from the SW (Bay of Palma) and NE (Bay of Alcúdia) coastlines produce a convective area with afternoon maximum cloud frequency amounts around 30.0% near the center of the island. This convergence zone is the main feature of the sea breeze in Mallorca as has been reported by González Márquez and Heredia (2001), Jansà and Jaume (1946), Ramis and Alonso (1988), Ramis et al. (1990), and Ramis and Romero (1995). González Márquez and Heredia (2001) studied a summer sea-breeze convective episode in the isle of Mallorca, with maximum precipitation of 24.0 mm on 24 May 2001. In addition, on 30 August 2004, an interesting convective event with maximum precipitation of 93.0 mm occurred over some areas of the SBCZ5 (Alomar-Garau and Grimalt-Gelabert 2006). We found a secondary SBCZ with afternoon maximum cloud frequency values above 30.0% over the Tramuntana mountain range, in the northwestern part of the isle. Its larger size and higher mountains play a key role in enhancing convergence in comparison with the isles of Ibiza (afternoon maximum cloud frequency of 19.0%) and Menorca (22.0%), where the line of Cu is weaker. The mean cloud frequencies from an array of 50 × 50 pixels are 14.2% (*NOAA-17*) and 16.4% (*NOAA-16*).

Cloud frequencies are also relatively moderate (cloud amount between 10.0% and 30.0%) over other active SBCZ along the Iberian Mediterranean area as shown in both the morning and afternoon composites. On the other hand, a lack of clouds (cloud cover <10.0%) is evident around areas of low elevation (Gibson and Vonder Haar 1990). For instance, coastal areas, bays (e.g., Gulf of Sant Jordi, Gulf of Valencia, Gulf of Alicante, Gulf of Mazarrón, Gulf of Almería, Bay of Palma, and Bay of Alcúdia), and river valleys (e.g., Ebro and Guadalquivir river valleys) are not favorable for sea-breeze–induced cloud development in relation to divergent flows over water bodies. In contrast to the Cape of Sant Antoni and Cape of Nao, which have mountain ranges near the coast, the region inland of the convex coastline of the Cape of Palos (between the Gulf of Alicante and Gulf of Mazarrón) is relatively flat and has little cloud cover (0.0%–5.0%) in the afternoon. This suggests that the uplift associated with mountains ranges supplements sea-breeze convection.

Additionally, an IR threshold at 12 μm of <273 K was used to determine the frequency and location of Cu and Cb clouds associated with the sea-breeze development. Although previous studies (e.g., Garreaud and Wallace 1997; Connell et al. 2001) employed a threshold technique of 235 K for delineating regions with deep convection, here we found that most of the Cu cloud tops associated with the sea breeze have temperatures around 250–273 K. Therefore, very little deep convection was identified by the 235-K threshold technique. We detected a lower frequency of colder clouds in the morning (maximum cloud frequencies ranging from 20.0% to 25.0% over the SCBZ1) and a higher frequency of

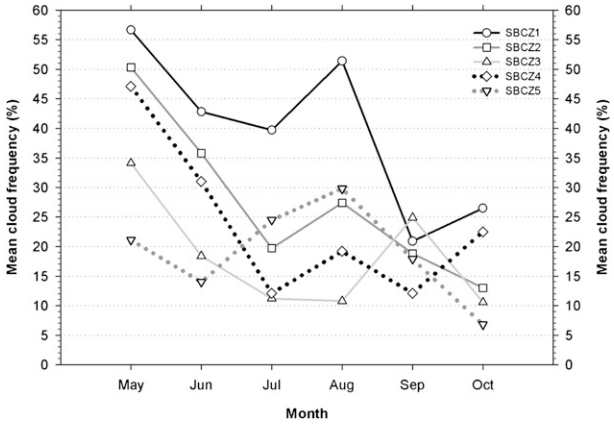

FIG. 4. Mean monthly cloud frequencies over each SBCZ for afternoon composites shown in Fig. 3.

colder clouds in the afternoon (maximum cloud frequencies ranging from 35.0% to 40.0% over the SBCZ1), which is a result of the convective processes along the sea-breeze fronts.

b. Monthly cloud frequency composites

Figure 3 displays cloud frequency composites for each month studied. Composites from May to October show a marked intermonthly cycle on sea-breeze cloudiness over the study area, even though the year 2004 could be unusual in the long-term climatology of the study area. May (Fig. 3a) is the cloudiest month with a mean cloud frequency (averaged between the five SBCZ) of 33.6% and 41.9% for the morning and afternoon orbits, respectively. June (Fig. 3b) represents the next cloudiest month with mean cloud frequency values ranging from 14.8% for *NOAA-17* to 28.4% for *NOAA-16*. The anticyclonic subsidence associated with the Azores high pressure system, in which the vertical development of the convection is less active (Millán et al. 2005), produces an overall low mean cloud frequency in July (Fig. 3c) with 11.7% (*NOAA-17*) and 21.4% (*NOAA-16*). This is a distinctive feature in mid- and high latitudes during summertime, and has been shown in cloud climate studies (e.g., Karlsson 2003). A secondary peak of mean cloud frequency is found in August (Figs. 3d, 4) with 18.5% and 27.7% for morning and afternoon composites, respectively. This secondary maximum is correlated with the weakening of the subtropical subsidence and the increasing occurrence of polar air masses at the midtroposphere, especially during the second half of August (e.g., Martín-Vide and Olcina-Cantos 2001). The maturing of isolated summer storms at the SBCZ is favored by the presence of a pool of cold air aloft (upper trough; Millán et al. 2005). A gradual decrease in frequency is found in September (Fig. 3e; 12.8% and 18.9%), whereas the sea-breeze front is barely discernible in October (Fig. 3f; 10.8% and 15.9%) due to fewer hours of sunshine and consequently weak local circulations along the Mediterranean coast.

The intermonthly cycle was verified by computing monthly mean cloud frequencies for afternoon composites over the 50×50 pixels array for each SBCZ (Fig. 4). The overall month-to-month variability presented above is shown in the SBCZ1, the SBCZ2, and the SBCZ4. A secondary peak of cloud frequency takes place in September for the SBCZ3. Finally, the SBCZ5 shows a different month-to-month pattern with July (24.5%) and August (29.8%) being the cloudiest months.

c. Onshore versus offshore wind regime cloud frequency composites

Regimes 1–4 (NE to E and SE to S; hereinafter onshore flows) and 5–8 (SW to W and NW to N; hereinafter offshore flows) in Table 2 were grouped to contrast the impact of wind direction (onshore versus offshore), which theoretically expresses different sea-breeze cloud patterns. Under onshore synoptic flows (Figs. 5a,b), clouds are widespread and there is higher cloud cover on mountains away from the coast (e.g., Iberian system mountains, lower plateau, and central mountain ranges). This is due to the increase of moisture from the Mediterranean Sea. In contrast, under offshore background synoptic flows (Figs. 5c,d), sea-breeze convergences are distinctly visible as thin lines of clouds and located parallel to and close to the eastern shore of the IP.

Onshore flows develop low cloud amounts in the morning (Fig. 5a), whereas sea-breeze fronts and inland convection grow for the afternoon composites (Fig. 5b). Consequently, large differences between morning and afternoon mean cloud amounts were detected for all onshore SBCZ, in particular for the SBCZ1 (23.0%). The cloud amount detected in the 50×50 pixel squares for each SBCZ is misleading in terms of isolating the clouds associated with the sea-breeze front. It includes clouds formed as a result of the sea-breeze front as well as clouds formed by other mechanisms because of the increase of moisture into the region. We expect that onshore large-scale winds weaken sea breezes by decompressing the horizontal land–sea temperature gradient parallel to the coastline, leading to fewer clouds at the sea-breeze front. However, onshore winds supply moisture from the Mediterranean Sea and enhance the chance of thunderstorms in the eastern mountainous areas of the IP, particularly during the afternoon. Once formed, these storms tend to migrate toward the western part of the IP under onshore winds aloft.

On the other hand, offshore background flows develop high amounts of sea-breeze cloudiness during the morning orbits (Fig. 5c) and, therefore, small differences

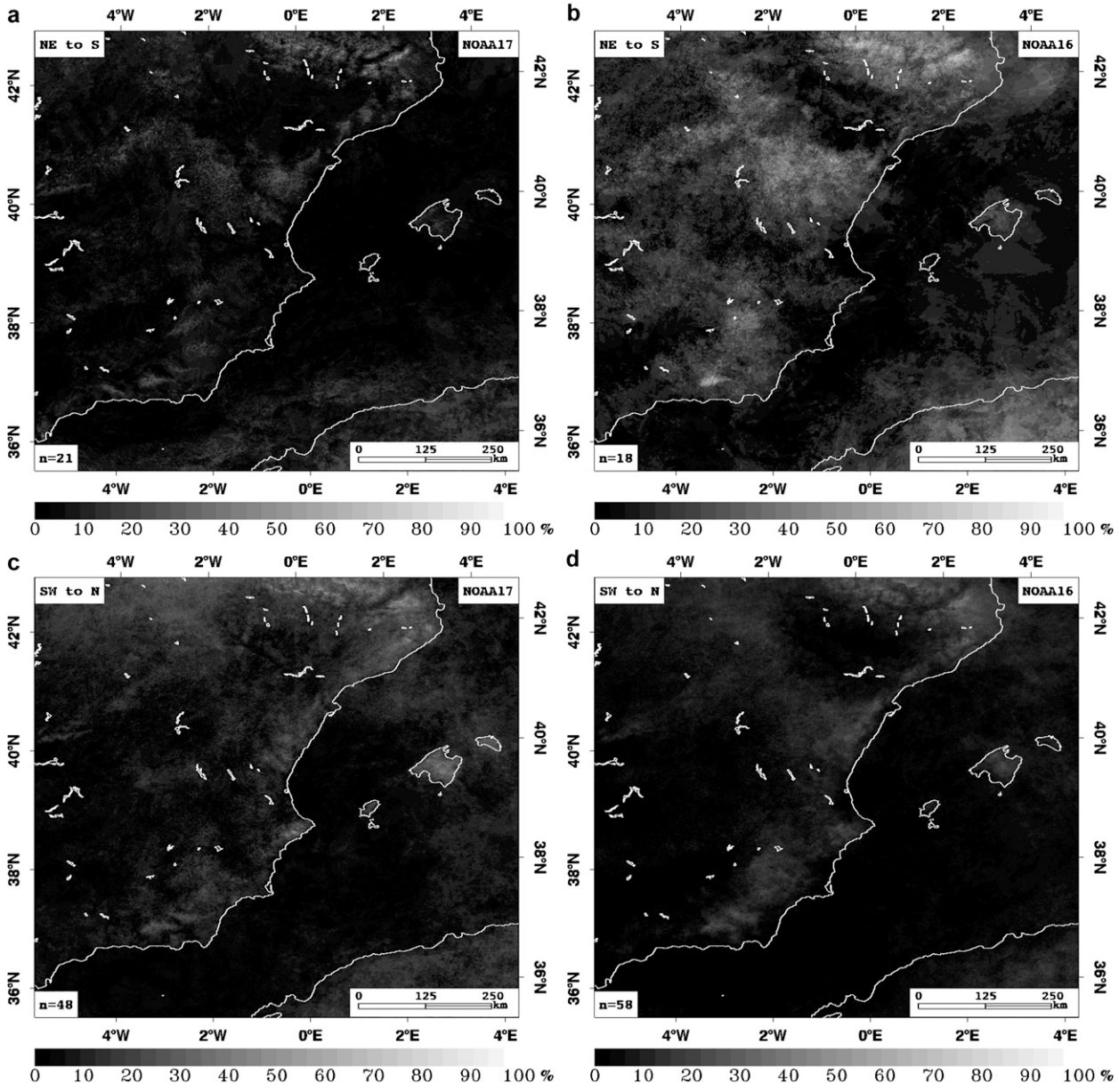

FIG. 5. As in Fig. 2, but for morning and afternoon composites under (a),(b) 1–4 (NE to S; onshore) and (c),(d) 5–8 (SW to N; offshore) large-scale regimes summarized in Table 2.

between morning and afternoon (Fig. 5d) mean cloud amounts were detected. This is largely due to (i) the deep layer of heating, (ii) the compressed horizontal thermal gradient (e.g., Arritt 1993) and, consequently, (iii) the strong horizontal and vertical motions that sharpen the leading edge of sea breezes and produce convergence intensification (e.g., Atkins and Wakimoto 1997) during the morning. Offshore geostrophic flows tend to move sea-breeze convection toward the Iberian Mediterranean coast and the western Mediterranean basin during the evening.

d. Light–moderate versus strong wind regime cloud frequency composites

The effect of wind speed (light to moderate, i.e., ≤ 5 m s^{-1}, versus strong flows, i.e., >5 m s^{-1}) on sea-breeze cloud frequency patterns is also studied here. The frequently occurring sea-breeze fronts are observed during onshore light–moderate flows (combined regimes 1 and 3; Figs. 6a,b), whereas less convection develops under onshore strong winds aloft (combined regimes 2 and 4; Figs. 6c,d). The mean cloud frequency

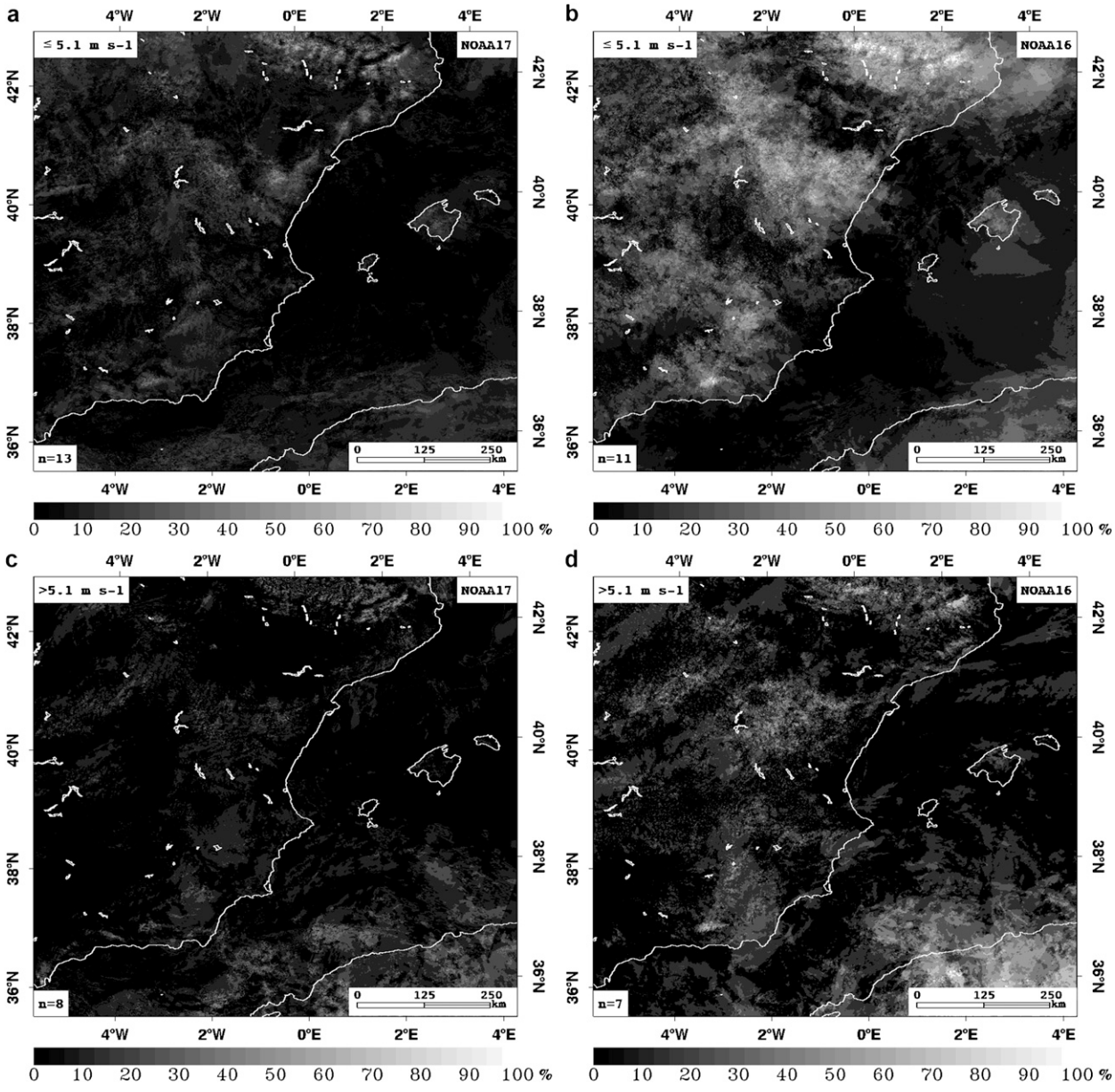

FIG. 6. As in Fig. 2, but for morning and afternoon composites under (a),(b) light–moderate (1 and 3 regimes) and (c),(d) strong (2 and 4 regimes) onshore large-scale flows summarized in Table 2.

for the afternoon composite (Fig. 6b) under onshore light–moderate flows is as follows: SBCZ1 (55.7%), SBCZ2 (44.6%), SBCZ4 (28.2%), and SBCZ5 (27.2%). For SBCZ3 (11.9%), convergence along the front results in less cloud cover under onshore flows. Onshore intensities, particularly light–moderate flows, display the largest differences between morning and afternoon mean cloud amounts for all SBCZ: SBCZ1 (32.6%), SBCZ2 (21.5%), SBCZ3 (7.7%), SBCZ4 (17.0%), and SBCZ5 (14.4%).

Nevertheless, offshore light–moderate winds (combined regimes 5 and 7; Figs. 7a,b) enhance sea-breeze convection (e.g., Atkins and Wakimoto 1997), which is widespread over the eastern part of the IP and organized in the center of the isle of Mallorca in relation to the collision of sea breezes (e.g., Azorin-Molina et al. 2007b). In contrast, offshore strong flows aloft (combined regimes 6 and 8; Figs. 7c,d) cause sea-breeze fronts to form near the coast, and for the eastern Pyrenees (SBCZ1 33.1%) and the isle of Mallorca (SBCZ2 27.0%) sea-breeze convection is intensified during the morning. In addition, light–moderate offshore flows show large differences between morning and afternoon mean cloud amounts in the

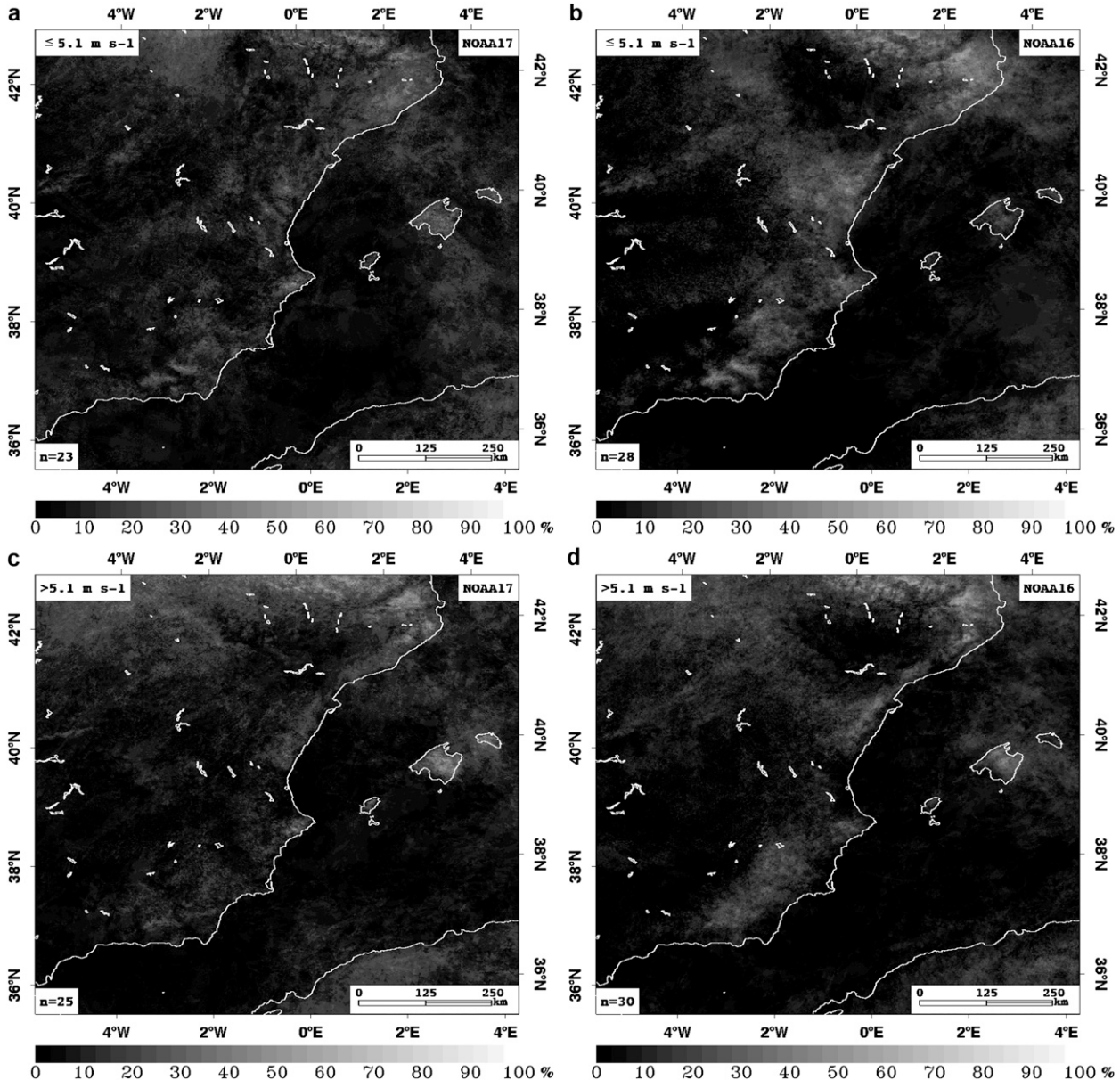

FIG. 7. As in Fig. 2, but for morning and afternoon composites under (a),(b) light–moderate (5 and 7 regimes) and (c),(d) strong (6 and 8 regimes) offshore large-scale flows summarized in Table 2.

SBCZ1 (13.9%), the SBCZ2 (11.7%), and the SBCZ3 (7.2%). Last, clouds at the sea-breeze front decrease from morning to afternoon for light–moderate (−6.9%) and strong (−3.8%) offshore flows in the SBCZ5.

In Table 3, we present cloud statistical parameters for the eight MLVW regimes tabulated in Table 2. Those interested in this subject could combine these statistics with the tools listed in the introduction for nowcasting active SBCZ under different flow components and intensities. Further sea-breeze cloud frequency maps for the eight MLVW regimes can be found in Azorin-Molina (2007). The cloud frequency composites presented here are available in color online (see http://rammb.cira.colostate.edu/research/satellite_climatologies/spain/).

4. Concluding remarks

The high-resolution cloud frequency composites allowed for identifying the location of five preferential SBCZ (hot spots) in relation to the shape of coastlines and terrain effects. Cloud statistical parameters for each SBCZ were tabulated here from the maps to quantify

TABLE 3. The mean cloud frequency (%) from an array of 50 × 50 pixels centered over the five frequently occurring SBCZ for the 6-month study period May–October 2004. Statistical parameters correspond to eight MLVW regimes (Reg) summarized in Table 2. Array dimensions (Fig. 1b): SBCZ1 (upper-left corner 42°35′N–2°09′E; lower-right corner 42°04′N–2°46′E); SBCZ2 (40°35′N–0°37′W; 40°04′N–0°00′); SBCZ3 (38°51′N–0°46′W; 38°20′N–0°09′W); SBCZ4 (37°28′N–3°15′W; 36°57′N–2°38′W); and SBCZ5 (39°55′N–2°36′E; 39°24′N–3°13′E).

	SBCZ1		SBCZ2		SBCZ3		SBCZ4		SBCZ5	
MLVW	N17	N16	N17	N16	N17	N16	N17	N16	N17	N16
Reg 1	33.5	64.9	41.2	62.1	8.7	17.3	24.1	42.9	22.5	22.1
Reg 2	10.5	21.7	10.3	8.5	4.4	13.2	2.5	9.1	0.6	1.7
Reg 3	16.9	42.7	10.2	21.5	0.8	4.8	1.3	9.2	5.8	32.7
Reg 4	6.0	22.8	2.5	4.9	0.7	10.1	11.2	23.7	2.8	10.9
Reg 5	39.5	63.9	30.3	52.7	13.2	37.1	19.5	33.4	26.9	22.7
Reg 6	38.4	45.3	16.1	26.9	9.5	11.0	7.0	14.7	18.6	16.7
Reg 7	11.0	26.1	7.3	17.4	17.7	13.6	5.8	12.8	19.4	12.6
Reg 8	20.8	23.7	6.4	9.1	16.8	23.6	18.7	34.4	40.2	39.4

sea-breeze convection under eight large-scale flows. The major findings of this manuscript are now summarized:

1) For NE to E and SE to S flows (regimes 1–4; onshore flows), low cloud amounts are observed at the leading edge of sea breezes during the morning. This is because sea breezes and onshore large-scale winds blow from the same direction, resulting in a weak surface convergence and upward vertical motion for convection development. In the onshore case, sea-breeze fronts have the most widespread distribution and thunderstorms tend to increase over adjacent mountain ranges not necessarily aligned with SBCZs (eastern Pyrenees and pre-Pyrenees ranges, the Iberian and the Betic system mountains, as well as over the central mountain ranges). Onshore flows weaken the distinctive sea-breeze discontinuity parallel to the eastern coast of the IP, provide low-level moisture from the Mediterranean Sea, and increase the chance of thunderstorms occurring over mountain ranges during the afternoon in relation to the convection trigger caused by strong anabatic valley breezes. Sea-breeze fronts and inland convection grow for the afternoon composites. For the onshore flows, large differences between morning and afternoon mean cloud amounts are detected. The frequently occurring sea-breeze fronts are observed during light–moderate ($\leq$5.1 m s^{-1}) environmental flows aloft. Strong (>5.1 m s^{-1}) winds, however, dramatically reduce low-level sea-breeze convergence.
2) For SW to W and NW to N flows (regimes 5–8; offshore flows), high cloud amounts are detected at the leading edge of sea breezes during the morning and afternoon. This can be explained by the large surface convergence between sea breezes and offshore flows, which strengthen vertical motion for convective development. In the offshore case, sea-breeze fronts are well organized parallel to the Iberian Mediterranean coast, as well as over the center of the isle of Mallorca, with thunderstorms developing along the SBCZs themselves. Offshore background winds cause high amounts of sea-breeze cloudiness during the morning orbits and therefore showers and thunderstorms can develop earlier over the five prominent SBCZ near the coast (particularly for SBCZ1, SBCZ3, and SBCZ5). Consequently, small differences between morning and afternoon mean cloud amounts are detected. It is found that light–moderate ($\leq$5.1 m s^{-1}) winds aloft strongly enhance low-level sea-breeze convergence and boundary layer convection. Strong (>5.1 m s^{-1}) synoptic-scale flows weaken the development of sea-breeze fronts, except for the NW to N regime. Differences between morning and afternoon mean cloud amounts are high for light–moderate winds, and negligible for strong offshore environmental flows.

Future research of sea-breeze cloud frequency composites will involve a combination of satellite, radar, and lightning data to study the intensity of sea-breeze storms, as well as boundaries and precipitation, with the aim in mind of addressing the findings concerning the frequency and location of deep convection. Geostationary imagery with higher temporal resolution will help to quantify where clouds develop throughout the day and to study the inland propagation of sea breezes over the area with high horizontal resolution. Additionally, further research should be carried out to set a threshold technique for the infrared satellite channels to determine the frequency and location of deep convection.

It was difficult to discern whether sea breezes were solely responsible for cloud development, as satellite images show that the actual orography (valley wind system) also has an impact on cloud cover. Further analysis should involve the use of several more years of added AVHRR data for representing sea-breeze cloud climatology, and

automatic weather stations to study if clouds observed by satellites are located with sea-breeze fronts passing certain stations. A comparison with geostationary imagery to monitor the progression of the sea-breeze front throughout the day would also help to address this question.

Finally, future climatological results from sea-breeze cloud frequency maps will be used to confirm trends toward reduced summer convective-orographic storms (Millán et al. 2005) in inland areas of the Iberian Mediterranean area and the Balearic Island. The precipitation associated with sea-breeze storms is very effective for the hydrological system (e.g., inland aquifers) and therefore changes in the development of sea-breeze fronts could have serious impacts over the region (i.e., exacerbate the drought conditions, water supply, agriculture, etc.).

Acknowledgments. This study was partially supported by a grant from Spain's Education and Science Ministry. The authors thank the INTA (CREPAD project; assistance provided by Angel Garcia-Sevilla) for AVHRR data, the Department of Atmospheric Science (College of Engineering, University of Wyoming) for sounding data, and Imanol Echave from ITT (Spain) for some ENVI4.2/IDL6.2 assistance. The Fundacion CEAM is financed by the Generalitat Valenciana and BANCAIXA. This research was undertaken in the frame of the CONSOLIDER-INGENIO 2010 Programme (GRACCIE project). Contributions from the second author were supported by NOAA Grant NA17RJ1228.

REFERENCES

Alomar-Garau, G., and M. Grimalt-Gelabert, 2006: Precipitaciones de verano y régimen de brisas en Mallorca (Summer rainfalls and breeze regime in Mallorca). *Proc. Fifth Conf. on Clima, Sociedad y Medio Ambiente,* Zaragoza, Spain, Spanish Climatological Association, 499–509.

Arritt, R. W., 1993: Effects of the large-scale flow on characteristic features of the sea breeze. *J. Appl. Meteor.,* **32,** 116–125.

Atkins, N. T., and R. M. Wakimoto, 1997: Influences of the synoptic-scale flow on sea breezes observed during CAPE. *Mon. Wea. Rev.,* **125,** 2112–2130.

Azorin-Molina, C., 2002: La formación de frentes de brisa activos en la comarca alicantina del Alto Vinalopó. El episodio atmosférico de 27 de abril de 2001 (The formation of active sea breeze fronts in the Alto Vinalopo district of Alicante. The atmospheric event of April 27th 2001). *Invest. Geogr.,* **29,** 109–130.

——, 2007: A climatological study of sea breezes in Alicante. Sea-breeze fronts over the Iberian Mediterranean area and the isle of Mallorca. Ph.D. thesis, University Institute of Geography, University of Alicante, 288 pp.

——, B. H. Connell, and R. Baena-Calatrava, 2007a: A new APOLLO daytime over land algorithm for computing convective cloud composites over the Iberian Peninsula and Balearic Islands. *Eighth European Conf. on Applications of Meteorology,* Abstract EMS2007-A-00542, El Escorial, Spain, EMS.

——, J. A. Guijarro, R. Baena-Calatrava, and A. Jansà, 2007b: Sea-breeze convergence and convective cloud frequencies from AVHRR data over Mallorca Island. *Eighth European Conf. on Applications of Meteorology,* Abstract EMS2007-A-00541, El Escorial, Spain, EMS.

——, A. Sanchez-Lorenzo, and J. Calbo, 2009: A climatological study of sea breeze clouds in the southeast of the Iberian Peninsula (Spain). *Atmósfera,* **22,** 33–49.

Bachmann, M., and J. Bendix, 1992: An improved algorithm for NOAA-AVHRR image referencing. *Int. J. Remote Sens.,* **13,** 3205–3215.

Baena-Calatrava, R., 2002: Automated georeference of NOAA-AVHRR images (in Spanish). High Technical College, University of Jaen, Jaen, Spain, 92 pp.

Bechtold, P., J.-P. Pinty, and P. Mascart, 1991: A numerical investigation of the influence of large-scale winds on sea breeze and land breeze type circulations. *J. Appl. Meteor.,* **30,** 1268–1279.

Blanchard, D. O., and R. E. López, 1985: Spatial patterns of convection in south Florida. *Mon. Wea. Rev.,* **113,** 1282–1299.

Brush, R. J., 1988: The navigation of AVHRR imagery. *Int. J. Remote Sens.,* **9,** 1491–1502.

Callado, A., and R. Pascual, 2002: Storms in front of the mouth rivers in north-eastern coast of the Iberian Peninsula. *Fourth Plinius Conf. on Mediterranean Storms,* Abstract PLC04-A-00026, Pollentia, Spain, European Geophysical Society.

——, and ——, 2005: Diagnosis and modelling of a summer convective storm over Mediterranean Pyrenees. *Adv. Geosci.,* **2,** 273–277.

Connell, B. H., K. J. Gould, and J. F. W. Purdom, 2001: High-resolution *GOES-8* visible and infrared cloud frequency composites over northern Florida during the summers 1996–1999. *Wea. Forecasting,* **16,** 713–724.

Damato, F., O. Planchon, and V. Dubreuil, 2003: A remote sensing study of the inland penetration of sea-breeze fronts from the English Channel. *Weather,* **58,** 219–225.

Derrien, M., B. Farki, L. Harang, H. LeGléau, A. Noyalet, D. Pochic, and A. Sairouni, 1993: Automatic cloud detection applied to NOAA-11/AVHRR imagery. *Remote Sens. Environ.,* **46,** 246–267.

Estoque, M. A., 1962: The sea breeze as function of the prevailing synoptic situation. *J. Atmos. Sci.,* **19,** 244–250.

Garreaud, R. D., and J. M. Wallace, 1997: The diurnal march of convective cloudiness over the Americas. *Mon. Wea. Rev.,* **125,** 3157–3171.

Gibson, H. M., and T. H. Vonder Haar, 1990: Cloud and convection frequency over the southeast United States as related to small scale geographic features. *Mon. Wea. Rev.,* **118,** 2215–2227.

González-Márquez, J., and M. A. Heredia, 2001: Sea-breeze convection in Mallorca (in Spanish). *Proc. Fifth National Symp. of Forecasting,* Madrid, Spain, Spanish Meteorological Agency, 1–6.

Gould, K. J., and H. E. Fuelberg, 1996: The use of GOES-8 imagery and RAMSDIS to develop a sea breeze climatology over the Florida Panhandle. Preprints, *Eighth Conf. on Satellite Meteorology and Oceanography,* Atlanta, GA, Amer. Meteor. Soc., 100–104.

Ho, D., and A. Asem, 1986: NOAA AVHRR image referencing. *Int. J. Remote Sens.,* **7,** 895–904.

INM, 2004: *Calendario Meteorológico 2004*. Spanish Meteorological Institute, Ministry of Environment, Madrid, Spain, 294 pp.

——, 2005: *Calendario Meteorológico 2005*. Spanish Meteorological Institute, Ministry of Environment, Madrid, Spain, 313 pp.

Jansà, J. M., and E. Jaume, 1946: The sea breeze regime in the Mallorca island (in Spanish). *Rev. Geofís.,* **19,** 304–328.

Jenkinson, A. F., and F. P. Collison, 1977: An initial climatology of gales over the North Sea. Synoptic Climatolology Branch Memo. 62, Meteorological Office, Bracknell, United Kingdom, 18 pp.

Kalnay, E., and Coauthors, 1996: The NCEP/NCAR 40-Year Reanalysis Project. *Bull. Amer. Meteor. Soc.,* **77,** 437–471.

Karlsson, K. G., 1996: Cloud classifications with the SCANDIA model. Swedish Meteorological and Hydrological Institute Reps. 67 on Meteorology and Climatology, Norrköping, Sweden, 36 pp.

——, 2003: A 10 year cloud climatology over Scandinavia derived from NOAA Advanced Very High Resolution Radiometer imagery. *Int. J. Climatol.,* **23,** 1023–1044.

Klitch, M. A., J. F. Weaver, F. P. Kelly, and T. H. Vonder Haar, 1985: Convective clouds climatologies constructed from satellite imagery. *Mon. Wea. Rev.,* **113,** 326–337.

Koch, S. E., and C. A. Ray, 1997: Mesoanalysis of summertime convergence zones in central and eastern North Carolina. *Wea. Forecasting,* **12,** 56–57.

Kriebel, K. T., G. Gesell, M. Kästner, and H. Mannstein, 2003: The cloud analysis tool APOLLO: Improvements and validations. *Int. J. Remote Sens.,* **24,** 2389–2408.

Kwiatkowski, J. J., 1999: Observations and analysis of the New Jersey sea breeze. M.S. thesis, The Graduate School, Rutgers University, 79 pp.

Lana, X., G. Fernandez-Mills, and A. Burgueño, 1995: Daily precipitation maxima in Catalonia (north-east Spain): Expected values and their spatial distribution. *Int. J. Climatol.,* **15,** 341–354.

Martín-Vide, J., and J. Olcina-Cantos, 2001: *Climas y Tiempos de España (Weather and Climates of Spain)*. Alianza, 264 pp.

Martínez, M. D., X. Lana, A. Burgueño, and C. Serra, 2007: Spatial and temporal daily rainfall regime in Catalonia (NE Spain) derived from four precipitation indices, years 1950-2000. *Int. J. Climatol.,* **27,** 123–138.

McPherson, R. D., 1970: A numerical study of the effect of coastal irregularity on the sea breeze. *J. Appl. Meteor.,* **9,** 767–777.

Millán, M. M., R. Salvador, E. Mantilla, and B. Artíñano, 1996: Meteorology and photochemical air pollution in southern Europe: Experimental results from EC research projects. *Atmos. Environ.,* **30,** 1909–1924.

——, ——, ——, and G. Kallos, 1997: Photo-oxidant dynamics in the Mediterranean Basin in summer: Results from European research projects. *J. Geophys. Res.,* **102D,** 8811–8823.

——, M. J. Estrela, and J. Miró, 2005: Rainfall components: Variability and spatial distribution in a Mediterranean area (Valencia region). *J. Climate,* **18,** 2682–2705.

Moreno, J. F., and J. Meliá, 1994: An optimum interpolation method applied to the resampling of NOAA AVHRR data. *IEEE Trans. Geosci. Remote Sens.,* **32,** 131–151.

Neumann, J., 1951: Land breezes and nocturnal thunderstorms. *J. Meteor.,* **8,** 60–67.

Olcina-Cantos, J., and C. Azorin-Molina, 2004: Sea-breeze fronts in the Spanish Levant region (in Spanish). *Estud. Geogr.,* **254,** 61–100.

Parada, M., A. Millán, A. Lobato, and A. Hermosilla, 2000: Fast coastal algorithm for automatic geometric correction of AVHRR images. *Int. J. Remote Sens.,* **21,** 2307–2312.

Pascual, R., 1999: Summer convection in Catalonia: An analysis using Meteosat IR imagery (in Spanish). *Proc. Fourth National Symp. of Forecasting,* Madrid, Spain, Spanish Meteorological Agency.

——, and A. Callado, 2002: Mesoanalysis of recurrent convergence zones in north-eastern Iberian Peninsula. *Proc. Second European Conf. on Radar Meteorology,* Delft, Netherlands, ERAD, 59–64.

——, ——, and M. Berenguer, 2004: Convective storm initiation in central Catalonia. *Proc. Third European Conf. on Radar Meteorology,* Visby, Island of Gotland, Sweden, ERAD, 464–468.

Pautz, M., 1971: Meso-scale analysis and forecasting. Technical Procedures Branch, Weather Analysis and Forecasting Division, NOAA/NWS, 39 pp.

Petterssen, S., 1956: *Weather Analysis and Forecasting,* Vol. 1: *Motion and Motion Systems.* 2nd ed., McGraw-Hill, 428 pp.

Pielke, R., 1974: A three-dimensional numerical model of the sea breezes over South Florida. *Mon. Wea. Rev.,* **102,** 115–139.

Planchon, O., F. Damato, V. Dubreuil, and P. Gouery, 2006: A method of identifying and locating sea-breeze fronts in northeastern Brazil by remote sensing. *Meteor. Appl.,* **13,** 225–234.

Purdom, J. F. W., 1976: Some uses of high-resolution GOES imagery in the mesoscale forecasting of convection and its behavior. *Mon. Wea. Rev.,* **104,** 1474–1483.

Ramis, C., and S. Alonso, 1988: Sea-breeze convergence line in Majorca. A satellite observation. *Weather,* **43,** 288–293.

——, and R. Romero, 1995: A first numerical simulation of the development and structure of the sea breeze in the island of Mallorca. *Ann. Geophys.,* **13,** 981–994.

——, A. Jansà, and S. Alonso, 1990: Sea breeze in Mallorca. A numerical study. *Meteor. Atmos. Phys.,* **42,** 249–258.

Roebeling, R. A., A. J. Feijt, and P. Stammes, 2006: Cloud property retrievals for climate monitoring: Implications of differences between Spinning Enhanced Visible and Infrared Imager (SEVIRI) on METEOSAT-8 and Advanced Very High Resolution Radiometer (AVHRR) on *NOAA-17. J. Geophys. Res.,* **111,** D20210, doi:10.1029/2005JD006990.

Saunders, R. W., 1986: An automated scheme for the removal of cloud contamination from AVHRR radiances over Western Europe. *Int. J. Remote Sens.,* **7,** 867–886.

——, and K. T. Kriebel, 1988: An improved method for detecting clear sky and cloudy radiances from AVHRR data. *Int. J. Remote Sens.,* **9,** 123–150.

Savijärvi, H., and M. Alestalo, 1988: The sea breeze over a lake or gulf as the function of the prevailing flow. *Beitr. Phys. Atmos.,* **61,** 98–104.

Simpson, J. E., 1994: *Sea Breeze and Local Wind*. Cambridge University Press, 234 pp.

Stowe, L. L., P. A. Davis, and P. E. McClain, 1999: Scientific basis and initial evaluation of the CLAVR-1 Global Clear/Cloud Classification Algorithm for the Advanced Very High Resolution Radiometer. *J. Atmos. Oceanic Technol.,* **16,** 656–681.

Strickler, M. W., 2003: Sea-breeze fronts and their role in convective initiation. North Carolina State University, Raleigh, North Carolina, 22 pp.

Terradelles, E., 1997: Main features of the distribution of the atmospheric electric activity in Catalonia and the surrounding Mediterranean area. *Proc. Int. Symp. on Cyclones and Hazardous Weather in the Mediterranean,* Palma de Mallorca, Spain, INM/WMO, 535–540.

Wakimoto, R. M., and N. T. Atkins, 1994: Observations of the sea breeze front during CAPE. Part I: Single Doppler, satellite, and cloud photogrammetry analysis. *Mon. Wea. Rev.,* **122,** 1092–1114.

Wilson, J. W., and W. E. Schreiber, 1986: Initiation of convective storms at radar-observed boundary-layer convergence lines. *Mon. Wea. Rev.,* **114,** 2516–2536.

Wilson, P., L. F. Bosart, D. Keyser, and T. Wasula, 2007: Warm-season lake-/sea-breeze severe weather in the Northeast. Preprints, *22nd Conf. on Weather Analysis and Forecasting/18th Conf. on Numerical Weather Prediction,* Park City, UT, Amer. Meteor. Soc., 7A.6. [Available online at http://ams.confex.com/ams/22WAF18NWP/techprogram/paper_123877.htm.]